Supporting Information

Selective Adsorption and Separation of C_6 Hydrocarbons: The Role of Structural Flexibility in Zeolitic Imidazolate Frameworks

Kevin Dedecker*, Martin Drobek*, Anne Julbe

Institut Européen des Membranes (IEM); CNRS, ENSCM, Univ Montpellier; Place Eugène Bataillon; 34095 Montpellier; France

*Email: kevin.dedecker@umontpellier.fr

*Email: martin.drobek@umontpellier.fr

1. Material Characterization

Powder X-ray diffraction (PXRD) patterns were collected using a Malvern Panalytical X-Pert PRO diffractometer equipped with Cu Kα radiation (λ = 1.5418 Å). The instrument was operated at 45 kV and 25 mA, with data acquired over a 2θ range of 5° to 50°.

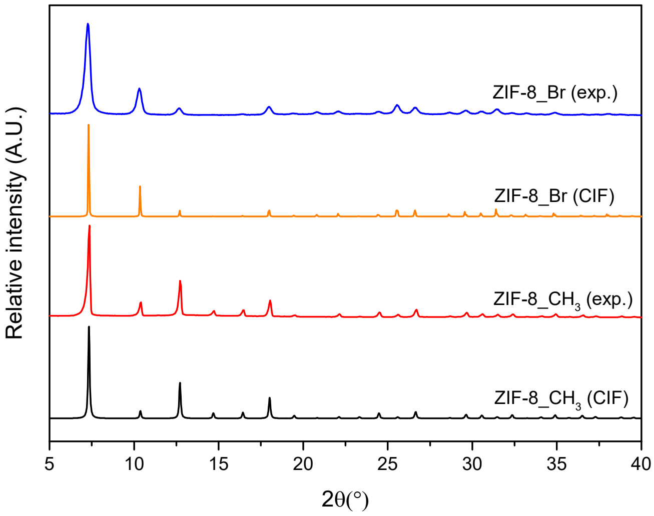

Figure S1. Comparison of experimental and simulated PXRD patterns for ZIF-8_CH$_3$ and ZIF-8_Br.

Nitrogen adsorption-desorption isotherms were measured at 77 K using a Micromeritics ASAP 2020 surface area and porosity analyzer. Prior to analysis, samples were degassed under vacuum at 200°C for 12 hours to remove adsorbed contaminants and moisture.

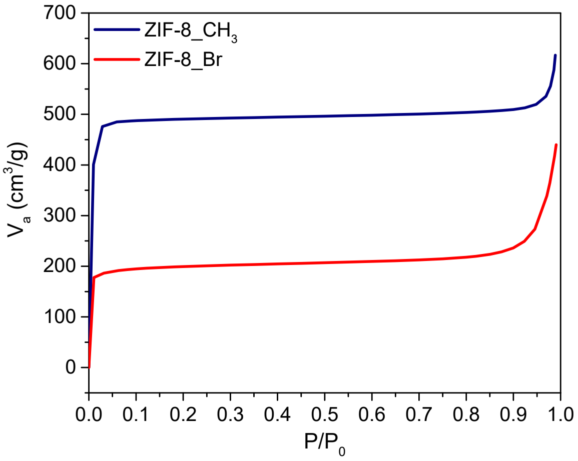

Figure S2: N_2 adsorption/desorption isotherms of ZIF-8_CH$_3$ and ZIF-8_Br at 77K.

Thermogravimetric analysis (TGA) was performed using a TA Instruments SDT 2960 analyzer. Samples were heated from 25°C to 800°C at a constant rate of 5°C/min under a dry air atmosphere. The mass loss was recorded as a function of temperature.

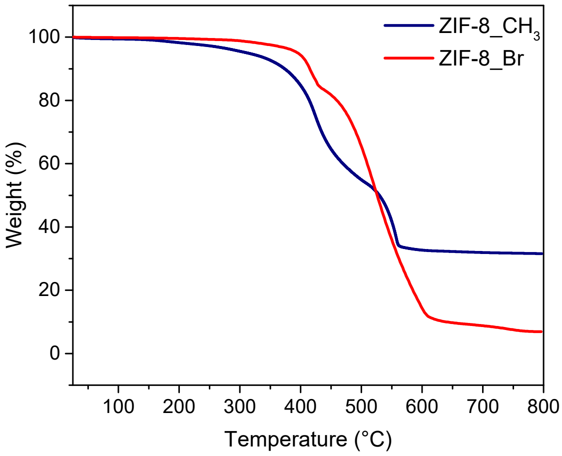

Figure S3: Thermogravimetric analysis of ZIF-8_CH_3 and ZIF-8_Br.

Fourier-transform infrared (FTIR) spectroscopy was conducted using a Nicolet Nexus FT-IR spectrometer in reflection mode. Spectra were acquired over the range of 4000-600 cm^{-1} with a resolution of 4 cm^{-1}. The observed spectral features were compared with those previously reported in the literature[1].

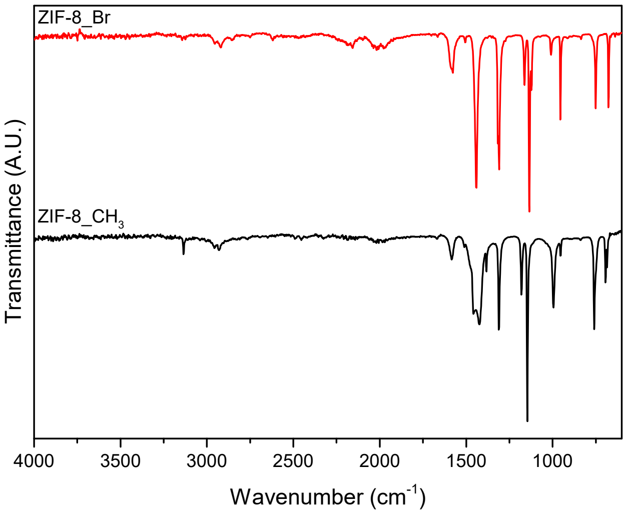

Figure S4. Comparison of FTIR experimental spectra for ZIF-8_CH_3 and ZIF-8_Br.

2. Computational Details

---

[1] R. Yagi and T. Ueda, Phys. Chem. Chem. Phys., 2023, 25, 20585–20596.

2.1 Model of ZIF structures

Mulliken partial charges for the ZIF structures were calculated using periodic density functional theory calculations. These computations were performed using the CASTEP simulation package, which employs plane-wave basis sets for electronic structure calculations in periodic systems.

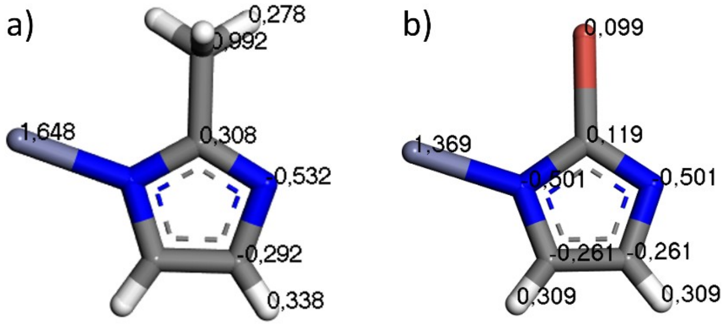

Figure S5. Partial charge assignments on the structure of a) ZIF-8_CH_3 and b) ZIF-8_Br.

The interactions within the system were modeled using a combination of the Universal Force Field (UFF) and the Dreiding Force Field. Host-guest interactions were specifically described using Lennard-Jones (L-J) potentials. This approach allows for a comprehensive description of both intramolecular and intermolecular forces in the studied systems.

Table S1. Force Field parameters for MOF structures.

Type	Force Field	σ (A)	ε/kB (K)
Zn	UFF	2.46155	62.3992
C	Dreiding	3.47299	47.8562
H	Dreiding	2.84642	7.64893
N	Dreiding	3.03315	48.1581
Br	Dreiding	186.191	3.51905

2.2 Model of Adsorbate Molecules

Molecular models for n-hexane, benzene, and cyclohexane were constructed using compound-specific force field parameters. The n-hexane model employed the TraPPE-UA (United Atoms) force field, representing each CH_x group as a neutral sphere and allowing for carbon chain flexibility. Benzene was modeled using the TraPPE-EH (Explicit Hydrogen) force field, which explicitly includes hydrogen atoms and incorporates charged pseudo-atoms to accurately represent its rigid aromatic structure. Unlike the flexible n-hexane model, benzene was treated as a rigid molecule due to its stable aromatic ring. Cyclohexane was simulated as a ring of CH_2 beads in a chair conformation, following the configuration described by Muñoz-Muñoz.

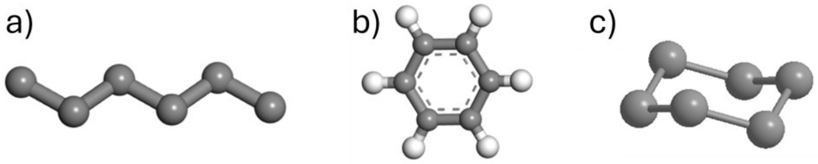

Figure S6. Illustration of adsorbates represented by a) TraPPE-UA (n-hexane), b) TraPPE-EH (Benzene) and c) the model of Muñoz-Muñoz (Cyclohexane).

Table S2. List of L-J potentials for benzene, n-hexane and cyclohexane.

Type	σ (A)	ε/kB(K)	Charge
C_$_{Ar}$	3.55	35.24	-0.115
H_$_{Ar}$	2.42	15.03	0.115
CH$_3$_sp$_3$	108.0	3.76	0
CH$_2$_sp$_3$	56.0	3.96	0
CH$_2$_Cy	3.497	87.009	0.0

Table S3. Bond lengths, angles and positions of pseudo-atoms for benzene and cyclohexane molecules.

Benzene				
C-C length: 1.392 Å				
C-H length: 1.08 Å				
C-C-C angle: 120°				
H-C-C angle: 120°				
# Pseudo-atom	**Type**	*x*	*y*	*z*
0	C_benz	0	0	0
1	C_benz	1.392	0	0
2	C_benz	2.088	1.20551	0
3	C_benz	1.392	2.41101	-0.0012
4	C_benz	0	2.41101	-0.00167
5	C_benz	-0.696	1.20551	-6.8061E-4
6	H_benz	-0.54	-0.93531	4.4182E-4
7	H_benz	1.932	-0.93531	0.00129
8	H_benz	3.168	1.20551	6.2273E-4
9	H_benz	1.932	3.34632	-0.00125
10	H_benz	-0.54	3.34632	-0.0026
11	H_benz	-1.776	1.20551	-8.5731E-4

Cyclohexane			
CH$_2$-CH$_2$ length: 1.527 Å			
CH$_2$-CH$_2$-CH$_2$ angle: 111°			
# Pseudo-atom	x	y	z
0	-1.3715	-0.4792	-0.2349
1	-0.2707	-1.4273	0.2349
2	1.1008	-0.9481	-0.2349
3	1.3715	0.4792	0.2349
4	0.2707	1.4273	-0.2349

5	-1.1008	0.9481	0.2349

3. Molecular Modelling

The spatial distribution of adsorbates within the ZIF cavities was visualized using density plots derived from Grand Canonical Monte Carlo simulations. These simulations were conducted at 20°C and consisted of an equilibration phase comprising 1x10^7 Monte Carlo steps, followed by a production phase of 1x10^4 steps. The resulting average occupation profiles provide insight into the preferential adsorption sites and molecular arrangements of the studied adsorbates within the MOF structures.

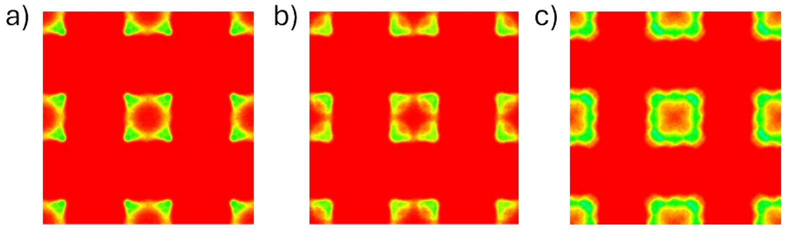

Figure S7. 2D representation of presence density in ZIF-8_CH_3 of: a) n-hexane, b) cyclohexane and c) benzene.

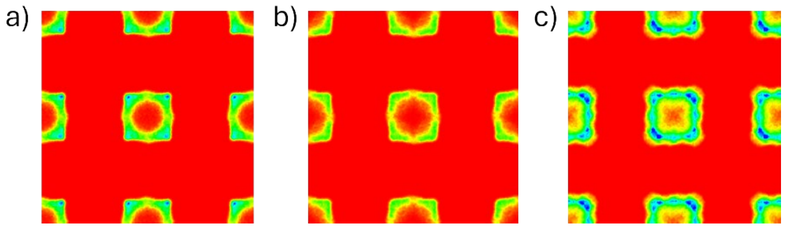

Figure S8. 2D representation of presence density in ZIF-8_Br of: a) n-hexane, b) cyclohexane and c) benzene.

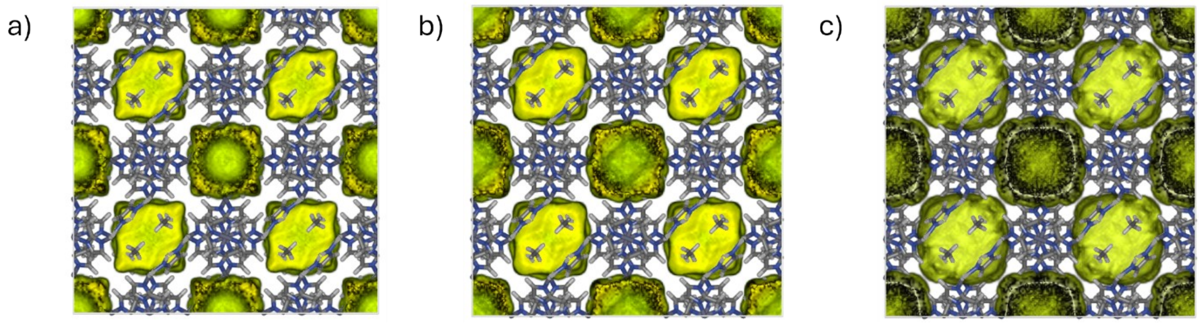

Figure S9. 3D representation of presence density in ZIF-8_CH_3 of: a) n-hexane, b) cyclohexane and c) benzene.

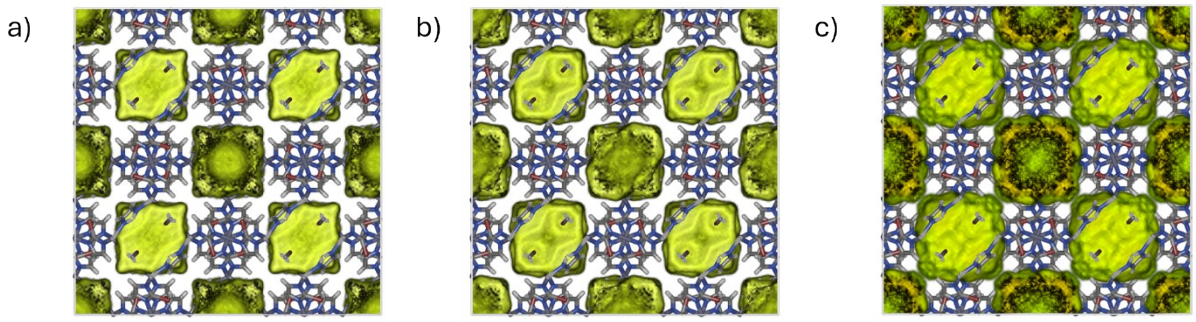

Figure S10. 3D representation of presence density in ZIF-8_Br of: a) n-hexane, b) cyclohexane and c) benzene.

4. Structural Analysis of ZIF Structures

The structural properties of ZIF structures, such as unit cell volume, pore-limiting diameter (PLD), largest cavity diameter (LCD), surface area (SA), and pore volume (Vp), were analyzed using Zeo++ software.

Table S4. Calculated structural features of ZIF-8_CH$_3$ and ZIF-8_Br including unit cell volume, pore limiting diameter (PLD), largest cavity diameter (LCD), surface area (SA) and pore volume (V_p) using Zeo++ software.

Structure	Unit cell volume (Å^3)	PLD (Å)	LCD (Å)	SA (m^2/g)	V_p (cm^3/g)
ZIF-8_CH$_3$	4904.42	3.42	11.4	1703	1.10
ZIF-8_Br	4985.25	3.39	10.5	660	0.31

5. IAST Fitting Parameters

The Ideal Adsorbed Solution Theory (IAST) was utilized to assess material performance using single-component adsorption isotherms. These isotherms were modeled with the Dual-Site Langmuir-Freundlich equation, as implemented in the IAST++ software.

Table S5. Dual-Site Langmuir-Freundlich fitting parameters for adsorption isotherms of benzene, cyclohexane and n-hexane in both ZIF-8_CH$_3$ and ZIF-8_Br structures at 293 K.

ZIF-8_CH$_3$	**Site A**			**Site B**			**R²**
	$q_{A,Sat}$	b_A	n_A	$q_{B,Sat}$	b_B	n_B	
n-hexane	19.0689	0.0451883	1.16629e-15	14.0072	3.88846	5.7628	0.999976
Cyclohexane	14.2061	5.02177	7.0222	6.65023	0.355735	0.812506	0.999718
Benzene	4.32712	5.43029	0.482449	2.02732	206.884	2.00039	0.999983

ZIF-8_Br	**Site A**			**Site B**			**R²**
	$q_{A,Sat}$	b_A	n_A	$q_{B,Sat}$	b_B	n_B	
n-hexane	23.9153	2.3946 e-09	3.7659	0.302644	49.082	0.966256	0.999347
Cyclohexane	1.51226	24.1864	1.53592	119.719	0.00431772	7.38545	0.999246
Benzene	2.23355	0.0821867	0.267705	1.11605	140.695	6.63689	0.999633